Long-Term Biomonitoring of Selenium and Arsenic Using Three Grass Species

Alice Goldstein-Plesser
Cold Regions Research and Engineering Laboratory
Anna Ulanova
Oak Ridge National Laboratory
Maxwell Lutz
Cold Regions Research and Engineering Laboratory
Julie Parno
Cold Regions Research and Engineering Laboratory
Nicole Wuerslin
Cold Regions Research and Engineering Laboratory
Korynna Rankin
Cold Regions Research and Engineering Laboratory
Jazmine Hawkins
Oak Ridge National Laboratory
Margaret Kurth
Engineer Research and Development Center
Samuel Beal
Cold Regions Research and Engineering Laboratory
Timothy Cary
Cold Regions Research and Engineering Laboratory
Jeffrey Summers
United States Department of Energy
Taylor Rycroft
Engineer Research and Development Center
Franz J. Lichtner
Franz.J.Lichtner@usace.army.mil

Cold Regions Research and Engineering Laboratory

Research Article

Keywords: Biomonitoring, coal combustion residuals (CCR), unmanned aerial vehicle (UAV), spectral imaging, grass as a bioindicator

Posted Date: August 22nd, 2025

DOI: https://doi.org/10.21203/rs.3.rs-7160388/v1

Additional Declarations: No competing interests reported.

Version of Record: A version of this preprint was published at Environmental Monitoring and Assessment on December 9th, 2025. See the published version at https://doi.org/10.1007/s10661-025-14719-7.

Long-Term Biomonitoring of Selenium and Arsenic Using Three Grass Species

Alice Goldstein-Plesser[1], Anna Ulanova[2], Maxwell Lutz[1], Julie Parno[1], Nicole Wuerslin[1], Korynna Rankin[1], Jazmine Hawkins[2], Margaret Kurth[4], Samuel Beal[1], Timothy Cary[1], Jeffrey Summers[3], Taylor Rycroft[4], and Franz J. Lichtner[1*]

[1] U.S. Army Engineer Research and Development Center, Cold Regions Research and Engineering Laboratory, 72 Lyme Road, Hanover, NH, USA, 03755.

[2] Oak Ridge Institute for Science and Education, 1299 Bethel Valley Rd, Oak Ridge, TN, USA, 37830.

[3] U.S. Department of Energy, Office of Fossil Energy and Carbon Management, 1000 Independence Avenue SW, Washington, DC, USA 20585

[4] U.S. Army Engineer Research and Development Center, Environmental Laboratory, 3909 Halls Ferry Rd, Vicksburg, MS, USA, 39180.

* Corresponding Author: Franz.J.Lichtner@usace.army.mil

Alice Goldstein-Plesser: Alice.W.Goldstein-Plesser@usace.army.mil
Maxwell Lutz: maxplutz01@gmail.com
Julie Parno1: julie.t.parno@erdc.dren.mil
Nicole Wuerslin: Nicole.A.Wuerslin@usace.army.mil
Korynna Rankin: Korynna.E.Rankin@usace.army.mil
Samuel Beal: Samuel.A.Beal@usace.army.mil
Timothy Cary: Timothy.J.Cary@usace.army.mil
Franz Lichtner: Franz.J.Lichtner@usace.army.mil

Anna Ulanova: Anna.A.Ulanova@usace.army.mil
Jazmine Hawkins: Jazmine.L.Hawkins@usace.army.mil

Margaret Kurth: margaret.h.kurth@usace.army.mil
Taylor Rycroft: taylor.e.rycroft@usace.army.mil

Jeffrey Summers: jeff.summersfm@yahoo.com

Abstract

Coal-fired power plant
s produce a waste stream of coal combustion residuals (CCRs) which are typically disposed of in landfills and surface impoundments that must be monitored to ensure that hazardous constituents such as arsenic (As) and selenium (Se) do not escape into the surrounding environment. Traditional methods for monitoring surface impoundments are highly resource-intensive and largely manual, posing a significant cost challenge for the stakeholders responsible for them. The use of grass species as bioindicators may offer a more efficient, cost-effective, and sustainable method for long-term monitoring of CCR impoundments. In this study, we sought to determine whether three species of grass could serve as effective bioindicators for detecting changes in As and Se soil contamination profiles and provide an evaluation of three technologies used for evaluating plant health. *Lolium perenne*, *Panicum virgatum*, and *Paspalum notatum* were treated with As or Se and monitored with a spectroradiometer and multispectral camera to detect a spectral response to the chemical stress. We then expanded this study to a field scale to determine if our results would translate to an environmentally relevant scale. Unmanned aerial vehicle

(UAV) results suggested *Lolium perenne* was efficient in determining whether CCR was present in soils but lacked sensitivity to differentiate between low and high loadings. Monthly sampling also revealed that metal concentration in plant tissue decreased as plants underwent senescence. Data collected by UAV proved to be the most proficient method of determining a dose response.

Key words

Biomonitoring, coal combustion residuals (CCR), unmanned aerial vehicle (UAV), spectral imaging, grass as a bioindicator

Introduction

Approximately 38% of power is generated by coal worldwide, with the United States ranked among the top three nations for coal combustion (Zierold & Odoh, 2020). U.S. utility-scale net electricity generation by coal in 2023 was 16.2% according to Energy Information Agency (U.S EIA, 2024). Coal-fired power plants produce a waste stream of coal combustion residuals (CCRs) which are typically disposed of in landfills and surface impoundments. CCRs include fly ash, bottom ash, boiler slag, and material from flue gas desulfurization (Zierold & Odoh, 2020). CCRs can contain harmful heavy metals and other compounds that are persistent, bioaccumulate, and toxic, posing potential human and ecological health risks if containment structures leak or rupture (Haskins et al., 2017; Pudasainee et al., 2020). High concentrations of selenium (Se) and arsenic (As) in CCRs are of particular concern due to their toxicity and their ability to bioaccumulate in the environment (Fu et al., 2018; Zwolak, 2020). Both As and Se can be carcinogenic, cytotoxic, genotoxic, and at low concentrations Se may also enhance As toxicity (Huang et al., 2019; Sun et al., 2021).

The United States Environmental Protection Agency (U.S. EPA) regulates disposal of CCRs in landfills and surface impoundments to ensure they are properly managed and do not pollute waterways, groundwater, drinking water, and air. In April 2024, the EPA expanded its national minimum requirements to include inactive or legacy surface impoundments which are more likely to be unlined, unmonitored and, therefore, considered more prone to leaks and structural problems than units that are currently in service (U.S. EPA, 2024). Traditional methods for monitoring surface impoundments (e.g., installing monitoring wells and regularly sampling groundwater) are highly resource-intensive and largely manual, posing a significant cost challenge for power facilities and grid operators with responsibility for these newly regulated inactive surface impoundments. The considerable cost requirements of long-term monitoring, coupled with the significant human health and ecological hazards posed by CCRs should they leach into the environment, necessitate more efficient and sustainable methods for long-term monitoring of CCR impoundments and their surrounding environments.

One potential alternative for continuous and long-term monitoring of CCR impoundments is the use of plants as bioindicators. Bioindicators are living organisms that respond to environmental change in a manner that is detectable and interpretable. Numerous species have served as successful bioindicators. However, plants, specifically grasses, may be uniquely suited for long term continuous monitoring at CCR surface impoundments. In addition to grasses abundant nature in a variety of different climates, they create a clear visual dose-response signal when exposed to certain contaminants (Carignan & Villard, 2002). Grasses have a variety of stress responses when exposed to environmental stressors – such as the heavy metals in CCR – including morphological changes (e.g., deviations in leaf development and abnormal changes in height) and chemical changes (e.g., changes in pigment composition, moisture content, nutrient uptake and metabolism) (Mishra et al., 2020). Leaf chlorophyll concentration is a commonly used indicator of grass health since chlorophyll is the most abundant pigment found in photosynthetic cells and can change in abundance when plants are stressed (Singhal et al., 2019). Response to heavy metal stress causes changes in photosynthetic plant pigments and water content. This can alter the spectral signature of above ground plant biomass, providing a "barcode" that can be read with spectral imaging technology (Lasalle et al, 2020).

Imaging spectrometers, such as multispectral cameras, collect spatially resolved spectral data in many narrow wavelengths throughout the visible and near-infrared portions of the electromagnetic spectrum (Bellante et al., 2013; Cheshkova, 2022). The spectral responses of plants to stress or changes in the environment can be captured using these devices. Thus, multispectral cameras have been mounted on greenhouse rails (Thomas et al., 2018) and on unmanned aerial vehicles (UAVs) (Neupane & Baysal-Gurel, 2021) to detect disease in agricultural plants. The resulting spectral data are often summarized using empirical vegetation indices, enabling mapping of vegetation state related to specific physiological parameters (Barton, 2012; Lassalle et al., 2020a).

To effectively use plants as bioindicators of CCR hazards, it is essential to understand the degree to which CCR, and the various toxic heavy metals within it, influence the spectral signature of plants. It is established that plants respond to the types of heavy metals present in CCR. Soybeans dosed with As exhibited a spectral shift of the chlorophyll absorption band, also known as the red edge (680 nm), to shorter wavelengths and higher reflectance in the 550-650 nm range (Milton et al., 1989). In contrast, soybean plants treated with Se had an inverse response, with the spectral position shifted to longer wavelengths and lower reflectance between 550-650 nm when compared with control plants (Milton et al. 1989). Bandaru et al. (2010) quantified the internal structural changes in the leaves of spinach plants coincident with spectral analysis (Bandaru et al., 2010).

The use of grasses as bioindicators of CCR deposits is an unexplored and novel avenue. A pot experiment was conducted, with a following field study based on the results of the former. In the pot experiment, we sought to determine whether three species of grass could serve as effective bioindicators for detecting changes in the As and Se soil contamination profiles of CCR surface impoundments and providing an approximation for the degree of contamination via stress-response relationships. Three different grass species were chosen to represent different climate types (cold and warm) as well as different carbon metabolism systems and chlorophyl content (C3 and C4 photosynthesis) (Gates et al., 2016; Lichtenthaler & Babani, 2022; Sage et al., 2015; Talukder & Saha, 2017). All experimental grasses have been shown to phytostabilize contaminants by immobilizing them in the soil's surface (Kacprzak et al., 2014; Koo et al., 2006). As and Se were chosen due to their highly toxic profile, representing trace CCR elements that are the most deleterious for bioindicator plants. The field study utilized plots dosed with CCR to validate that the controlled pot experiment could be expanded to a real-world scale. By applying differing intensities of CCR, we explored whether grasses can be used as a reliable bioindicator, and different technologies that can provide efficient and reliable detection. We also established a data processing pipeline to use spectral imaging to detect heavy metal stress in the environment.

Methods

Grass Cultivation

Pot experiments were conducted at the Cold Regions Research and Engineering Lab (CRREL) in Hanover, New Hampshire. Three grass species that have previously shown growth potential at ash impoundments in either cool or warm climates were selected: Perennial Ryegrass (*Lolium perenne*; cool climate adapted; hereafter referred to as "PRG"), Switchgrass 'Carthage', North Carolina Ecotype (*Panicum virgatum*; warm climate adapted; hereafter referred to as "SG"), and Argentine Bahia grass (*Paspalum notatum*; warm climate adapted; hereafter referred to as "Bahia"). Germination trials were conducted to calculate the seeding rate for each species. Each species was planted into double layered mesh trays (27.9 cm x 55.8 cm) which were lined with filter fabric to prevent the planting media from falling out while still allowing for drainage to occur.

To prepare for planting, each double layered mesh tray was filled with 9 kg of sterilized, dried, and sieved (10 mm) sand (Figure S1). Three double layered mesh 27.9 cm x 55.8 cm trays with sand were then placed into each large white containment tray (1.32 m x 0.71 m) in a block randomized layout (Figure S2). Double layered mesh trays within each containment system received 15 L of water. Trays sat for approximately 24 hours before seeds were planted so the sand planting media was sufficiently moist for seed germination. Seeds were planted at a rate of 0.024 g/in^2 (bahia), 0.005 g/in^2 (SG), and 0.0008 g/in^2 (PRG). The weighed seeds were planted onto the double layered mesh trays. The planting area of each doubled layered mesh tray was divided into three even sections, where the middle section was left unplanted so Se or As treatments could be applied directly to this section once plants germinated and reached a mature stage. Clear propagation domes (Jiffy, 27.9 cm x 55.8 cm x 6.35 cm) were placed over the trays to aid germination and stayed on till two weeks post-germination. Watering occurred three times per week, or as needed throughout the experiment, by a drip irrigation system emitting ~2.5 L in a 40-minute watering session.

Field experiments were performed in 6.1 m x 6.1 m growth plots. A temporary greenhouse was constructed over the plots to control moisture content and limit large temperature fluctuations. The greenhouse roofing was constructed of a single layer of 0.1524 mm clear plastic allowing for spectral collections to be taken of the plots without roof removal. PRG was chosen to seed the field plots due to its ability to grow in cooler climates since the field experiment took place in the fall months. Plots were seeded with 34.4 g/m^2 of PRG seed.

Contaminant Application and Sample Collection

Se and As exposure experiments for the pot experiments were conducted separately between June-August 2023 and August-December 2023, respectively. Four different treatments were applied to the grasses: 0 ppm, 5 ppm, 15 ppm, or 25 ppm of sodium selenate (for the Se exposure experiment) or sodium arsenate (for the As exposure experiment) solution. There were four replicates of each treatment for both Se and As experiments.

The first sample collection for each treatment group took place prior to treatment. The first collection, the Se treatment group, took place 53 days after the seed planting date for all three grass species. In the As treatment group, collection number 1, took place 90 days after planting the Bahia and 74 days after planting the PRG and SG. To initiate exposure, 1 L of treatment solution was applied to the middle section of each mesh tray.

The experiment sample collections included recording plant heights, collecting planting media where grass was growing, collecting vegetation cuttings, and taking spectral measurements with two cameras, and by a leaf clip/reflectance probe. A form of destructive sampling occurred for vegetation and planting-media sampling collections, where two samples were taken from each double layered mesh tray to create a composite sample. Each sample taken of vegetation and planting-media were ~0.5-1 g for later use in acid digestions. Recording of plant heights and taking spectral measurements were forms of non-destructive sampling. Sample collections that took place after application treatments of Se or As were as follows: sample collection number 2 was performed one day (24 hours) after treatment, collection number 3 was performed seven days after treatment, and collection number 4 was performed 28 days after treatment.

Field experiments were carried out at either control, "low," or "high" levels of CCR soil contamination (Supplemental Table 1). Each 6.1 x 6.1 m plot was divided into three, even sections (2.03 x 6.1 m) and CCR treatments were evenly spread across the growing area. "Low" treatments consisted of 3.66 kg/m^2 and "high" treatments were 10.99 kg/m^2. Treatments were covered with a 7.62 cm deep layer of sand prior and watered to lock in placement prior to seeding.

Metal Translocation Chemical Analysis

The pot experiment samples were dried in an oven at 75°C for 16 hours after collection for chemical analysis of As and Se concentration. Vegetation samples were then ground to 20 mm using a mill (Arthur H. Thomas Co.). Grasses collected during the UAS experiment were cut with sterilized scissors to ~20 mm. Samples of both cut vegetation and planting media were then weighed for acid digestion.

The chemical analysis followed EPA Method 3050B (U.S. EPA, 1996), requiring homogenized soil and plant tissues to be acid-digested on a hot block, which captured metals that could become environmentally available. Briefly, a 500 mg sub-sample of each material was weighed to the nearest 0.1 mg in polypropylene tubes (SCP Science), and then a total of 5 ml trace metal grade HNO_3 and 5 ml H_2O_2 were added over the course of repeated heating periods at up to 90°C for 2 hours. Digestates were diluted to 50 ml with Type I water and then aliquoted and diluted for analysis by inductively coupled plasma mass spectrometry (ICP-MS) or graphite furnace atomic absorption spectrometry (GFAAS; Perkin Elmer AAnylst 600). Quality control included method blanks, samples matrix-spiked to 10 mg/kg-sample, laboratory control samples spiked to 1 mg/kg-sample, and the standard reference materials NIST 2710a (Montana Soil), NIST 1547 (Peach Leaves), and NIST 1573a (Tomato Leaves). A method blank was included in each digestion, while the remaining QCs were run once per matrix. A subset of Se soil digestates were sent to the Trace Element Analysis laboratory at Dartmouth College for preliminary elemental analysis by ICP-MS. The remaining digestates were sent to the ERDC Environmental Laboratory for GFAAS analysis.

Chemical analysis of soils and plant collections for the field experiment followed a similar protocol. Sub-samples of homogenized soil (500 mg) and plant tissue (250 mg) were acid-digested following EPA Method 3050B28. Briefly, nitric acid (Fisher Trace Metal Grade), Type I water (Millipore IQ7000), and hydrogen peroxide (Fisher ACS-Grade) were added to polypropylene digestion vials in successive steps with heating up to 90°C and up to 2 hours. Digestates were dilute to 50 ml with Type I water and allowed to settle. Aliquots of the diluted digestates were further diluted 10-fold with Type I water in 15 ml polypropylene vials to 1% HNO3, and then they were analyzed by inductively coupled plasma mass spectrometry (ICP-MS; Thermo iCAP TQe) using single quadrupole mode with Kinetic Energy Discrimination (UHP grade helium) and triple quadrupole mode (research grade oxygen). Arsenic and selenium were measured in triple quadrupole mode using mass 75 to 91 and 78 to 94, respectively. Quantification used 5-9 point external calibration curves (Inorganic Ventures IV-71A), verified with a separate lot standard, and continuously verified every 10 samples with a mid-calibration standard. Yttrium-89 was the internal standard for As and Se in plant samples, and Indium-115 was used for As and Se in soil samples. Quality control included digestion triplicates, matrix spikes, laboratory control samples (LCS), and the NIST standard references materials (SRMs) 1547 (Peach Leaves), 1573a (Tomato Leaves), 2711a (Montana II Soil), and 1944 (New York/New Jersey Waterway Sediment).

Relative standard deviations (RSDs) from triplicate digestions of plants were 5% for As and 4% for Se. RSDs from triplicate digestions of soils were 4-23% for As and 25-37% for Se. Matrix spike recoveries of As and Se were 101-104% (n=2) in plants and 86-117% (n=4) in soil. LCS recoveries of As and Se were 97-101% (n=2) in plants and 94-104% (n=4) in soil. Recoveries from plant SRM certified values were 91-103% for As and 83-131% for Se (n=6). Recoveries from soil/sediment SRM CLP median (2711a) and certified (1944) values were 80-102% for As and 75-99% for Se (n=6).

Spectral Data Collection

Spectral data collections were coincident to the sample collection dates, occurring just prior to treatment and then 1-, 7-, and 28-days post-treatment. A spectroradiometer (HR-1024i field-portable spectroradiometer, SpectraVista Corporation (SVC)) and Headwall Co-aligned visible near infrared (VNIR) and shortwave infrared (SWIR) hyperspectral instrument (HSI) were used to characterize each plant's spectral signature. Reflectance was determined with the SVC using the ratio of the radiance of the plant to the radiance of a calibrated 99% Spectralon white reference panel. Measurements were performed at both plant and blade scale. At plant scale, two full-spectrum tungsten halogen lamps (ASD, Inc. Illuminator Lamps) were suspended over the tray for consistent lighting. The SVC was fitted with an 8-degree field of view (FOV) lens and mounted on a tripod with the lens placed 80 cm from the soil surface and approximately 70 cm above the estimated average plant height, resulting in a circular measurement area approximately 10 cm in diameter. For each double layered mesh tray, a reference scan was taken followed by 5 scans of the tray, with small shifts in tray position for each scan such that a slightly different sample was within the FOV for each. This allowed for capture of any variability in plant health within the individual double layered mesh tray. An SVC leaf clip and reflectance probe was used to capture the reflectance at the blade scale. For each scan, several blades of grass were clipped into the device and scanned. For each double layered mesh tray, a reference scan was completed followed by 4 blade scans.

Spectral Data Processing

<u>Spectroradiometer</u>

The spectroradiometer data was preprocessed using the SVC HR-1024i PC Data Acquisition Software (version 1.22.26) and Python 3.8.19. The SVC overlap removal and detector matching algorithm was applied to each file. The scans received an initial quality control by plotting and removing any unacceptable scans, such as those that were near zero reflectance or visibly affected by any variable lighting conditions. The mean reflectance of each tray for each collection was calculated using Python along with the standard deviation and 25th and 75th percentiles to provide a sense of the variability among the averaged scans. The scans were then compiled and exported to R [version 4.3.3] (R Core Team, 2023) for further data exploration. Normalized differences of the spectrograms between the 0 ppm and 25 ppm treatments were calculated, along with spectra visualizations of the different treatment types and species combinations. Principal Component Analysis (PCA) of spectroradiometer-derived vegetative indices was also conducted through the inclusion of on-site meteorological data to discern the driving forces of health degradation of the experimental grasses (Figure S3).

As similar process was completed in the field experiment. Cells C3 and C4 (Figure 4) were chosen for SVC scanning on single leaf scale and plant scale. NDVI was calculated for the cells using an average for red wavelengths (620-670 nm) and NIR wavelengths (842-876 nm).

$$NDVI = \frac{(NIR_{842-876\,nm} - R_{620-670\,nm})}{(NIR_{842-876nm} + R_{620-670\,nm})}$$

Raw SVC data was plotted for control, low, high groups across the wavelengths to see reflectance trends. All plotting was created using the R package ggplot2 [version 3.5.1] (Wickham, 2016).

<u>Multispectral Sensors</u>

Grasses grown in the field greenhouse were analyzed for NDVI by using UAS drone (Harris Aerial Carrier Hx8) on October 23rd, 11 weeks after seeding. Flight procedures were as follows: speed of drone ~2 m/s, height over greenhouse was 39 m using both a Headwall Hyperspectral Co-Aligned HP (Headwall Photonics) sensor and MicaSense Altum-PT (AgEagle Aerial Systems Inc.) multispectral sensor. Field greenhouse data was mosaicked by using of QgsRasterLayer feature from the core functionalities of QGIS [version 3.34.11] (QGIS Development Team, 2024). NDVI was calculated by using the Raster Calculator option of QGIS, using bands that correspond to red wavelengths (620 nm – 670 nm) and NIR wavelengths (842 nm-876 nm). Three coordinate points were chosen for each section within the cells that would appear in all collection dates and were used as center points to create a cropped square of the calculated NDVI raster, resulting in a sampled 0.2 m^2 area. The three squares for each section in a cell were used to calculate the average pixel value in the area as a proxy for average NDVI in the samples. The averages were calculated using the core QGIS capabilities such as QgsRasterLayer, and QgsRasterBandStats. SciPy's packages f_oneway and tukey_hsd were used to complete one-way ANOVA and the Tukey's honestly significant difference (HSD) test [version 1.15.3] (Vertanen et al, 2020).

Results and Discussion

As and Se Concentration in Soil and Plant Tissue

Soil and vegetation were chemically analyzed for As and Se concentrations throughout the experimental timeline (Figure 1). Soil As and Se content was monitored to both confirm the presence of As and Se at the dosed concentrations and track rates of metal leaching out of the system through successive water treatments. Plant As and Se concentrations were monitored to assess the relative translocation of metals into the plant tissue. Chemical analysis of As concentrations in the soil revealed that As was already present in high concentrations prior to treatment.

Analysis of As treated soils by ICP-MS showed no significant difference in As concentrations across all treatment concentrations or plant types (Table 1). This is not entirely surprising given the natural occurrence of As in mineral deposits in non-contaminated soils can naturally range from 0-100 ppm (Walsh et al., 1977). Despite the soil results, As uptake and accumulation in plants increased in a dose dependent manner over the course of the first 7 days across all treatments and plant types until reaching and maintaining a stable As concentration in the plant tissue until the final collection at Day 28 (Figure 1). Taken together, these results suggest As present in the control soils was not bioavailable for plant uptake and obscured the spike concentration of sodium arsenate. The As treatment in the form of arsenate (As(V)) is readily taken up by plants and likely led to the observed dose response in plant tissue.

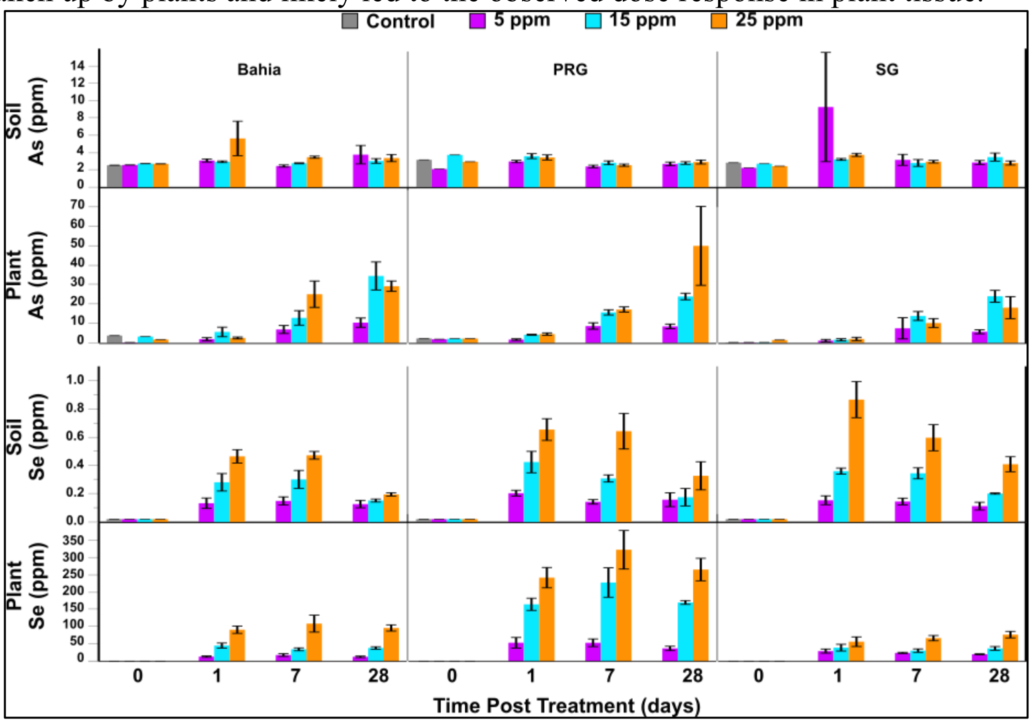

Figure 1: As and Se concentrations present in the soil and plant tissue as determined by ICP-MS and GFAAS. Error bars represent standard error of three replicate measurements.

Control soils all had Se concentrations below the detection limit of 40 ppb (Figure 1). The application of sodium selenate increased Se concentrations in a dose dependent manner at 24 hours post treatment; however, these concentrations were far lower than the dosed concentrations of 5, 15, and 25 ppm (Figure 1). The relatively low concentrations of Se in soil fractions suggest Se was retained in by adsorption of aqueous Se and the subsequent decrease over time was due to desorption modulated by both the plant and abiotic (temperature) environment. Soil concentrations of Se significantly changed overtime and between species, indicating that species sequestered selenium at different rates (Table 1). This significant difference between species is mainly driven by Bahia grass taking up less Se than both PRG and SG (Table 1). The average concentration of Se in Bahia soils from the 25-ppm treatment group was significantly lower than PRG and SG soils after 24 hours (Kruskal-Wallis test; p-value = 0.0498). Average Se levels in Bahia soils from the 25-ppm treatment groups remained consistently lower than PRG (< 30-50%) and SG soils (< 23-71%) over the 28-day experimental period (Figure 1).

Plant uptake of Se occurred in a dose dependent manner across all grass species (Figure 1). There was a significant difference between Se uptake across plant species, with PRG plants accumulating five times more Se than either Bahia or SG tissues over a 24-hour period (Figure 1 and Table 1). Within a given species, concentrations of plant-associated Se did not significantly change over time even as soil concentrations steadily decreased (Figure 1). This suggests that the decrease in Se in the soil fraction was likely due to water loss and desorption rather than loss due to plant uptake. The increase of Se in plant tissue can be attributed to grasses ability to accumulate and appropriate Se in low concentrations, leading them to be good candidates for phytostabilization (Schiavon et al, 2017). However, the plateau of Se concentrations can be explained that at high heavy metal exposure, plants can experience nutrient starvation through the disruption of nutrient uptake and enzymatic activity (Jiang et al., 2022; Umar et al., 2025).

Table 1. One way ANOVA of ICP-MS chemical analysis of metal translocation in both soil and plant samples. * Indicates a significant value <.05, ** <0.005, and *** <0.0005.

Treatment	Substrate	Group	df	F-value	p-value
As	Soil	Time	2	2.40	0.0710
		Treatment Concentration	3	0.27	0.8454
		Species	3	0.93	0.3971
	Plant	Time	2	1.64	0.1980
		Treatment Concentration	3	5.38	0.0017**
		Species	3	21.45	<0.0001**
Se	Soil	Time	2	13.94	<0.0001***
		Treatment Concentration	3	27.01	<0.0001***
		Species	3	1.89	0.1562
	Plant	Time	2	3.81	0.0120*
		Treatment Concentration	3	14.21	<0.0001***
		Species	3	29.97	<0.0001***

Arsenic speciation was performed at the end of the experiments in plant tissue to determine the form of As stored. The GFAAS analysis separated organic species monomethylarsonic acid (MMA), dimethylarsinic acid (DMA), and unretained organic-species tentatively labeled as arsenobetaine (AsB), as well as the inorganic species As(III) and As(V). Inorganic As species such as As(V) and As(III) are readily phytoavailable, with As(V) being considerably less toxic than As(III) and DMA, in that order (Meharg & Hartley-Whitaker, 2002). Arsenic speciation showed that inorganic As was the major As species present in the plant tissue, with As(V), the spiked form of As, representing the majority of inorganic species (Figure 2). Relatively small amounts of the organic species DMA and AsB were present at all dosage treatments across all plant species. There is no known mechanism of plant transformation of As(V) into organic As species (Zhao et al., 2009), indicating that the remaining As species reflect the concentrations of pre-existing As in the soil. No MMA was detected across all the samples (data not shown).

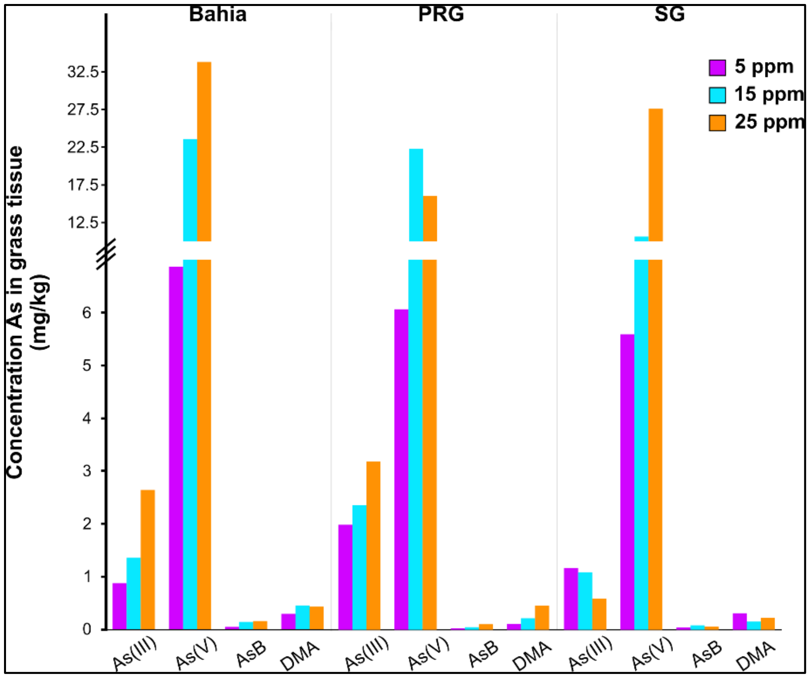

Figure 2: As speciation in plants 28 days post exposure. Values represent three biological replicates.

Spectroradiometer Analysis

Spectroradiometer (SVC) reflectance can be used to track plant activity over a broad range of wavelengths – encompassing the near infrared (NIR), visible, and near ultraviolet (NUV) (Figure S5). While SVC's do not capture data in a spatially resolved manner, it is a useful tool to quickly capture the average spectra from the field of view of the aperture. The Normalized Difference Vegetation Index (NDVI) is a broadly used vegetation index that calculates plant health using the NIR and red spectrum, indicative of the relative water content and chlorophyll concentration respectively (Evangelides & Nobajas, 2020; Lassalle et al., 2020b; Pettorelli et al., 2005). While other indices were tested using our dataset, the NDVI was the only index that consistently differentiated between healthy and dead plant material (Figure S4). The NDVI scale is –1 to 1, with values between –1 and 0 representing dead plants on inorganic material, unhealthy plants represented between 0 and 0.4, and values from 0.4 to 1 representing increasingly healthy plants. In the greenhouse study, NDVI values never exceeded 0.8 or fell below 0.3 although plants visually appeared healthy at the start of the experiment and, in some cases, were clearly dead by the end. A heatmap of the calculated NDVI values shows the degree to which plant health changed over the timeframe of the experiment according to plant species, metal treatment, and dose (Figure 3A).

There was no statistical correlation between As treatment dose and NDVI response for any of the grass species (Figure 3A). Figure 3A also displays all SG collections exposed to As, including the control, experienced a steady decline in NDVI over the 28-day period. This decline in SG health during the As treatment study was likely due to high temperatures in the greenhouse since control plants declined in health. In contrast, all Se treated grasses showed a decrease in NDVI as a function of increased Se treatment concentrations from days 0, 1, and 7 (Figure 3A).

At day 28, the SG and PRG plants exhibited low NDVI values independent of Se treatment dose, whereas Bahia continued to show a dose-dependent response to Se. The average spectra of Bahia clearly show a dose response as early as 24 hours post Se exposure, showing the reflectance deviating from control plants based on treatment – with this deviation from control becoming increasingly clear over the timeframe of the experiment (Figure 3B).

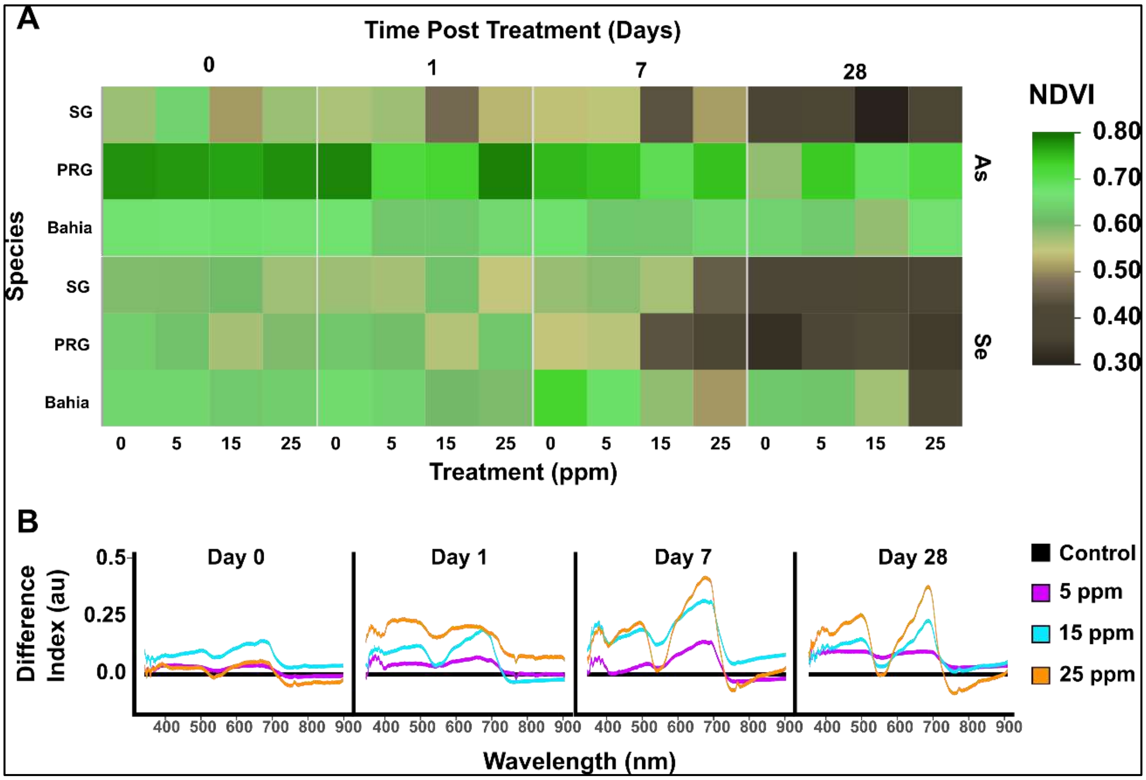

Figure 3: Analysis of SVC collection showing the resulting A) average NDVI of three replicate collections across all samples where lower values (brown) represent unhealthy or dead plants and higher values (green) represent healthy plants and B) average spectra of Bahia treated with Se and showing a clear dose response across the full range of treatments. SVC response is normalized to the control.

The differences in plant responses to As and Se can be explained by the role each element plays in plant development. At high levels of Se, selenoprotein structures are damaged as the amino acid cysteine is replaced by selenocysteine (Ali et al., 2021; Gupta & Gupta, 2017). Se toxicity can result in stunted root and plant growth, as well as induce the production of reactive oxygen species (ROS) (Somagattu et al., 2024). ROS cause damage to cell membranes and result in cell damage and oxidative stress due to an excess of hydroxyl radicals (Choudhury et al., 2017). However, at low concentrations, Se is an essential component of plant defense against abiotic stressors as seen with the selenoprotein glutathione peroxidase which reduces hydrogen peroxide to prevent damage to cellular machinery (Madhu et al., 2023). Additionally, at low concentrations Se has been found to improve photosynthetic rates, nutrient uptake, and growth (Ali et al., 2021; Gupta & Gupta, 2017). This might explain why PRG and SG had no significant difference in reflectance signature compared to the control group at lower Se treatments because the grasses were able to uptake Se into their tissue without exceeding a toxicity threshold.

As is not essential for plant health and can cause a wide variety of detrimental effects depending on its speciation (Abbas et al., 2018). One of the effects of As is the overproduction of hydrogen peroxide resulting in lipid peroxidation (Abbas et al., 2018; Rafiq et al., 2017). Due to the overall deleterious nature of As in plant systems, it can explain why the three grass species had an increased adverse response to As compared to Se.

Spectra collected with the SVC are not spatially resolved and thus include background spectra from the soil and other non-grass materials that may cross into the field of view of the collection window. Despite these qualifications, the resulting NDVI calculated from the collected SVC spectra reflect the observed changes in plant health over time, indicating that this method is sufficient for a quick capture of plant health. The NDVI is not sensitive enough to spectral changes to distinguish between plants stressed due to heat or pathogen pressure.

Comparing the chemical analysis with NDVI data, we can conclude that some grass species are better bioindicators of metal stress than others. While the chemical analysis confirms a dose response assimilation of contaminants in all grass species, not all grass species displayed a NDVI dose response. This could be due an increase in activation for antioxidant enzymes to resist impacts of heavy metal accumulation by removing ROS, thereby mitigating the detrimental effects on cell organelles without removing the heavy metal species themselves (Jiang et al., 2022). PRG and SG species have been known to respond to Se via phytoextraction by accumulating them in harvestable parts such as shoots, whereas Bahia lacked any notable heavy metal tolerance mechanism (Matichenkov, 2017). Thus, for a plant to be considered a good bioindicator, the plant species and mechanism response to heavy metals must be considered. Plants that have a well-established mechanism for phytoremediation are likely to be poor bioindicators as they have adaptations to maintain their health.

The pot experiment has revealed that dose response differs with grass species and that all grass species were more sensitive to Se treatments. Both Bahia and PRG were highlighted as the best candidates for further study as bioindicators as they both displayed relatively clear dose responses to Se and were generally more hardy plants than the SG species. For field scale studies we chose to use PRG, as this species is more cold hardy than Bahia and the field scale study was planned during colder autumn months (Keep et al, 2021).

Field Greenhouse NDVI Analysis

Multispectral drone collections were used to calculate an average NDVI score for each pixel for the entire field spectral collection (Figure 4). The NDVI calculated from the multispectral camera confirmed that cells with low and high concentrations of CCR have NDVI lower values, indicating that the grasses were less healthy compared to the control groups (Figure 4D). Control sections were found to be statistically different from both the low concentration sections (T-test: p= 1.62eE-4) and high concentration sections (T-test; p=6.80E-3). For cells 1-3, the condensation below the plastic film of the greenhouse resulted in patches of high reflectance. Cells 4 and 5 also displayed an increase in plant health as the concentration increased from low to high. The variability in response can be due to the composition of the CCR, which is a blend of several heavy metals including Lead and Chromium. Due to the heterogeneous content of the CCR applied to each section, the lack of consistency in NDVI results may be due to an uneven mix of the contaminant per cell. Cells 3 and 4 (Figure 4A) were located on either side of the overlapping plastic sheet used for the roofing. The overlap produced a noticeable shadow, which may have contributed to the plant health of the two cells. It is possible that the plastic overlap decreased light intake for the plants, hindering their growth.

The average NDVI calculations for control, low and high sections varied for SVC and multispectral collections and are shown in Figure 4E. Leaf scale depicts low concentrations as healthier plants than control and high concentration groups, contradicting the analysis completed on the multispectral collections. Overhead SVC data show plants being healthy at control, declining in health at low concentration, and improving at higher concentrations. Aerial multispectral collections showed a decrease in plant health with increasing CCR concentrations in the soil. Leaf scale is more accurate in assessing the health of the individual plant by avoiding analyzing bare soil in the background and can capture the vertical profile of CCR distribution within the grasses (Arellano et al., 2017). Leaf scale, however, fails to capture the variability that might occur within the sampled cell sections, potentially leading to mischaracterization of the plant response. Overhead SVC followed the multispectral collections more closely, which could be due to the capturing of background bare soil which lowers NDVI values. This inverse relationship between bare soil and NDVI can also result in overestimation of the impacts of stress caused by CCR (Lassalle et al., 2020b).

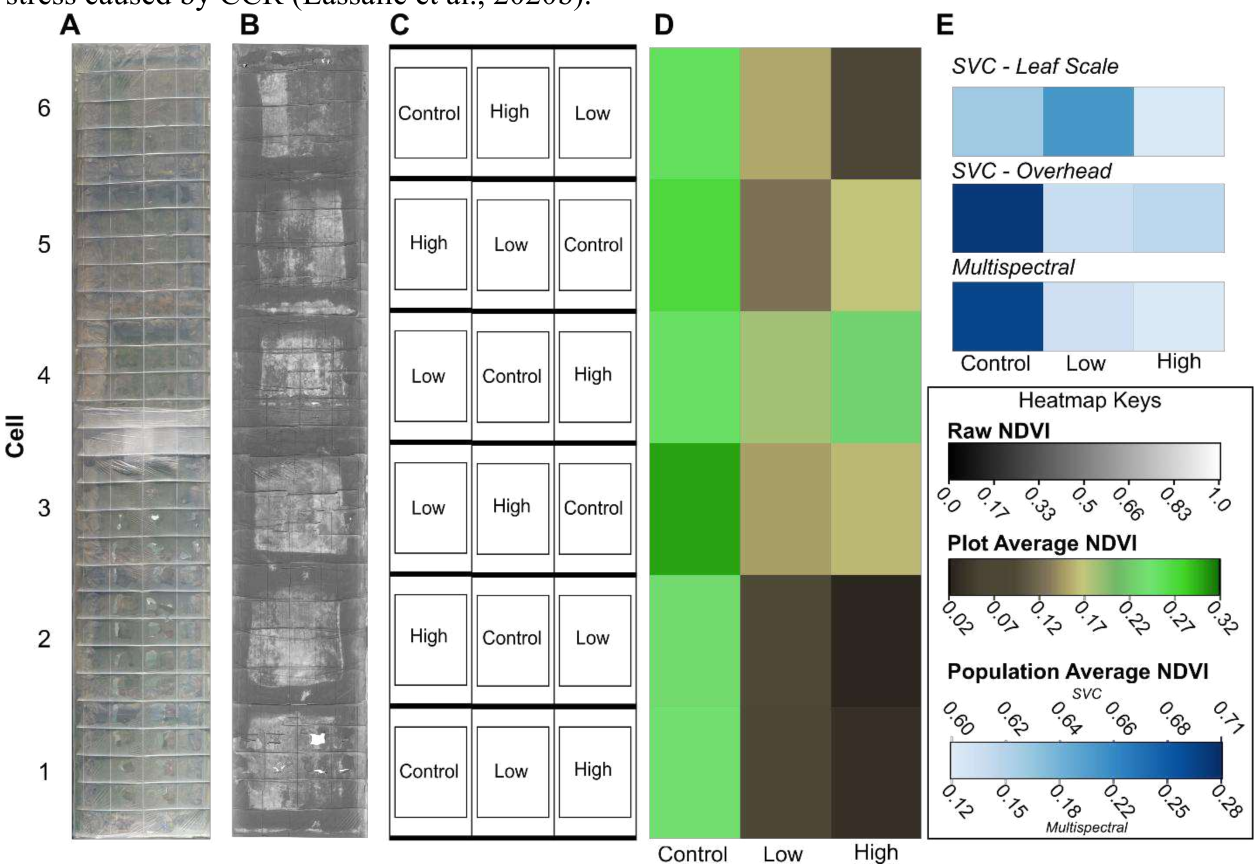

Figure 4. Field experiment assessment 78 days post seeding. (A) Orthorectified drone image over the length of the field greenhouse. (B) Raw NDVI values overlayed onto the orthorectified drone image. (C) Randomized treatment layout of each field plot. (D) Mean NDVI of all pixels in a given treatment for each field plot rearranged from left to right with increasing CCR treatment concentration. (E) Average NDVI per treatment across all plots measured by both SVC and multispectral cameras.

From the analysis of CCR impacts on plant health, multispectral imaging is the most effective method in determining a dose response in PRG grasses due to its ability to use the aerial vantage point and capture the entire field greenhouse. When considering large field monitoring, it is also the most feasible option as it avoids on-site scanning of individual plants or taking samples for extensive chemical testing. However, in a smaller and controlled environment, the SVC data collections were a reliable method of exploring NDVI trends.

The seasonal and CCR intensity impacts on grass health were explored as a function of time post seeding (TPS), sampling over the course of four months (Figure S6). Cells with the same treatments were binned together (Figure 5A). As time progressed, control plots went from being barren (0 TPS), to being covered with grass (2-3 TPS), and finally declining in plant health until the vegetation died at 4 TPS. Although these plants were grown in a greenhouse and shielded from harsh environmental swings, the field greenhouse was not heated and 4 TPS was collected during December, leading the plants to go dormant due to freezing temperatures. The NDVI averages were different between collections (One-way ANOVA , p-value= 9.35e-33) and significance confirmed by a Tukey's HSD test. Results show that 2 and 4 TPS were significantly different from 0 and 4 TPS, and there was no significant difference between 0 and 4 TPS (Table S2). This demonstrates that seasons significantly impacts average NDVI, regardless of treatment.

Further analysis, binning data by treatment, shows that both the low and high treatments were significantly different from control groups, while not significantly different from each other (Table S3). This indicates that PRG is effective in determining whether CCR is present in the soils but does not differentiate between low and high concentrations.

Chemical analysis of soil samples was completed for each TPS (Figure 5B-C). Kruskal-Wallis and Tukey's Post Hoc test was completed to examine if there was a significant difference between collections and treatment levels across the soil and plant samples after verifying that the dataset did not have a normal distribution (Table S4). There was no significant difference between the soil concentration profiles for As and Se across TPS and treatment types, indicating that there was insignificant plant uptake and minimal leaching through in the test plots.

Chemical analysis for plant tissue revealed no significant difference between low and high treatments but significantly different from the control groups (Figure 5 D-E and Table S5). Interestingly, while there is a significantly higher concentration of As in the treated plots from control, plant tissues are not significantly different at either two or four months TPS.

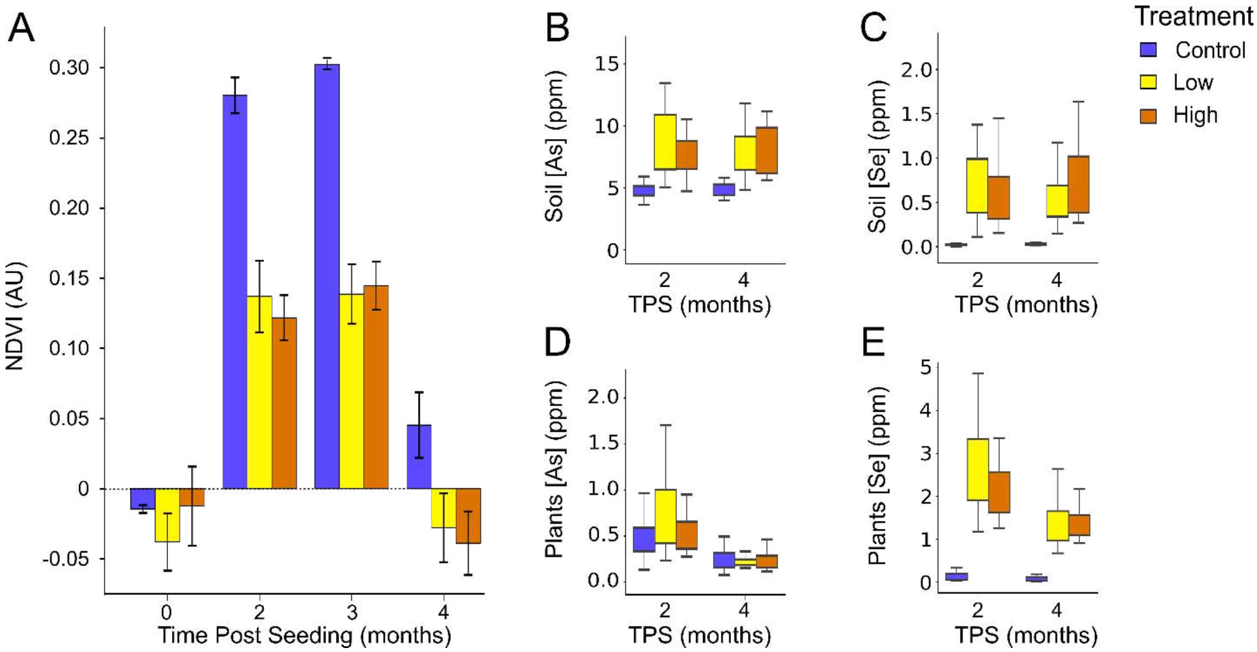

Figure 5. PRG responses to CCR treatment over time by treatment condition. Data represent all 6 test plots as biological replicates. (A) Average NDVI collected via multispectral drone. Error bars represent standard error. Soil concentration of As (B) and Se (C) at two and four months' time post seeding (TPS). Grass tissue concentrations of As (D) and Se (E) at two and four months TPS.

There was no analysis done on below-ground biomass, therefore the accumulation of heavy metals in roots during the translocation process of roots-to-shoots was not accounted for. The decrease in metal concentration in plant tissue between the two months of sampling coincides with the decrease in plant health. Plants undergoing senescence have been shown to increase metal mobilization from dying leaves to roots, which could potentially explain the decrease in metal concentration between 2 and 4 TPS (Maillard et al, 2015). While the concentration differences between the collection times are insignificant, further studies need to be conducted to determine how translocation factors might change with seasonality by calculating the metal concentration in roots (Masolta et al, 2023). Discrepancy between As and Se scales for plant tissue could be explained by Ca, Mg, and P rich soils decreasing As adsorption (Li et al, 2021). Soils used for the experiment were calcareous due to the prevalence of the limestone bedrock in the region (Beaumont, 1942).

Results from this investigation, suggest that it is advisable for military installations and CCR impoundments to monitor CCR distribution and degradation through aerial imaging given that appropriate grass species are used. Bahia and PRG grasses have shown to be good bioindicator candidates in certain contexts, with factors such as temperature and contamination types influencing plant response. Further studies should be conducted over a prolonged period to determine the maximum contaminant loading concentration in plants, as well as plant-soil translocation mechanisms for other contaminants. It is estimated that between 2000 and 2020, 2.4 trillion tons of CCR was produced, 1.1 trillion reused and 1.1 trillion disposed (Deonarine et al., 2023). CCR disposal sites are especially vulnerable to intensive rainfalls, flooding, or natural disasters which could cause CCR to be introduced into surface waters and groundwater (Foulds et al., 2014). In 2019, 91% of U.S. coal-fired power plants with regulated landfills have been found to have unsafe levels of ash components in downgradient wells (Petrović & Fiket, 2022). Current monitoring practices are centered around rigorous surface water sampling campaigns and computing Water Quality Index to ensure heavy metal pollution meets compliance standards (Petrović & Fiket, 2022; Ruhl et al., 2012). The most prominent tool for CCR assessment is U.S EPA's Leaching Environmental Assessment Framework (LEAF) that estimates leachability under various environmental and site disposal conditions (Da Silva et al., 2018). LEAF methods rely on leachate samples in order to calculate innate sample qualities such pH, liquid to solid ratios, as well as a slew of EPA laboratory methods which can be costly and time-consumptive for active monitoring (Thorneloe et al., 2017). Further steps in bioindicators research should focus on developing novel unintrusive frameworks which can track CCR fate in protected waters to predict accumulation sites for monitoring and risk assessments.

Funding Declaration

This research was funded by US Department of Energy, Office of Fossil Energy and Carbon Management. Order # A2305-089-096-043856

-

References

Abbas, G., Murtaza, B., Bibi, I., Shahid, M., Niazi, N. K., Khan, M. I., Amjad, M., Hussain, M., & Natasha. (2018). Arsenic Uptake, Toxicity, Detoxification, and Speciation in Plants: Physiological, Biochemical, and Molecular Aspects. *International Journal of Environmental Research and Public Health*, *15*(1), 59. https://doi.org/10.3390/ijerph15010059

Ali, W., Zhang, H., Junaid, M., Mao, K., Xu, N., Chang, C., Rasool, A., Wajahat Aslam, M., Ali, J., & Yang, Z. (2021). Insights into the mechanisms of arsenic-selenium interactions and the associated toxicity in plants, animals, and humans: A critical review. *Critical Reviews in Environmental Science and Technology*, *51*(7), 704–750. https://doi.org/10.1080/10643389.2020.1740042

Arellano, P., Tansey, K., Balzter, H., & Boyd, D. S. (2017). Field spectroscopy and radiative transfer modelling to assess impacts of petroleum pollution on biophysical and biochemical parameters of the Amazon rainforest. *Environmental Earth Sciences*, *76*(5), 217. https://doi.org/10.1007/s12665-017-6536-6

Bandaru, V., Hansen, D. J., Codling, E. E., Daughtry, C. S., White-Hansen, S., & Green, C. E. (2010). Quantifying arsenic-induced morphological changes in spinach leaves: Implications for remote sensing. *International Journal of Remote Sensing*, *31*(15), 4163–4177. https://doi.org/10.1080/01431161.2010.498453

Barton, C. V. M. (2012). Advances in remote sensing of plant stress. *Plant and Soil*, *354*(1–2), 41–44. https://doi.org/10.1007/s11104-011-1051-0

Bellante, G. J., Powell, S. L., Lawrence, R. L., Repasky, K. S., & Dougher, T. A. O. (2013). Aerial detection of a simulated CO2 leak from a geologic sequestration site using hyperspectral imagery. *International Journal of Greenhouse Gas Control*, *13*, 124–137. https://doi.org/10.1016/j.ijggc.2012.11.034

Carignan, V., & Villard, M.-A. (2002). Selecting indicator species to monitor ecological integrity: A review. *Environmental Monitoring and Assessment*, *78*(1), 45–61. https://doi.org/10.1023/A:1016136723584

Cheshkova, A. F. (2022). A review of hyperspectral image analysis techniques for plant disease detection and identif ication. *Vavilov Journal of Genetics and Breeding*, *26*(2), 202–213. https://doi.org/10.18699/VJGB-22-25

Choudhury, F. K., Rivero, R. M., Blumwald, E., & Mittler, R. (2017). Reactive oxygen species, abiotic stress and stress combination. *The Plant Journal*, *90*(5), 856–867. https://doi.org/10.1111/tpj.13299

Da Silva, E. B., Li, S., De Oliveira, L. M., Gress, J., Dong, X., Wilkie, A. C., Townsend, T., & Ma, L. Q. (2018). Metal leachability from coal combustion residuals under different pHs and liquid/solid ratios. *Journal of Hazardous Materials*, *341*, 66–74. https://doi.org/10.1016/j.jhazmat.2017.07.010

Deonarine, A., Schwartz, G. E., & Ruhl, L. S. (2023). Environmental Impacts of Coal Combustion Residuals: Current Understanding and Future Perspectives. *Environmental Science & Technology*, *57*(5), 1855–1869. https://doi.org/10.1021/acs.est.2c06094

Evangelides, C., & Nobajas, A. (2020). Red-Edge Normalised Difference Vegetation Index (NDVI705) from Sentinel-2 imagery to assess post-fire regeneration. *Remote Sensing Applications: Society and Environment*, *17*, 100283. https://doi.org/10.1016/j.rsase.2019.100283

Foulds, S. A., Brewer, P. A., Macklin, M. G., Haresign, W., Betson, R. E., & Rassner, S. M. E. (2014). Flood-related contamination in catchments affected by historical metal mining: An unexpected and emerging hazard of climate change. *Science of The Total Environment*, *476–477*, 165–180. https://doi.org/10.1016/j.scitotenv.2013.12.079

Fu, B., Hower, J. C., Dai, S., Mardon, S. M., & Liu, G. (2018). Determination of Chemical Speciation of Arsenic and Selenium in High-As Coal Combustion Ash by X-ray Photoelectron Spectroscopy:

Examples from a Kentucky Stoker Ash. *ACS Omega*, *3*(12), 17637–17645. https://doi.org/10.1021/acsomega.8b02929

Gates, R. N., Quarin, C. L., & Pedreira, C. G. S. (2016). Bahiagrass. In L. E. Moser, B. L. Burson, & L. E. Sollenberger (Eds.), *Agronomy Monographs* (pp. 651–680). American Society of Agronomy, Crop Science Society of America, Soil Science Society of America. https://doi.org/10.2134/agronmonogr45.c19

Gupta, M., & Gupta, S. (2017). An Overview of Selenium Uptake, Metabolism, and Toxicity in Plants. *Frontiers in Plant Science*, *7*. https://doi.org/10.3389/fpls.2016.02074

Haskins, D. L., Hamilton, M. T., Jones, A. L., Finger, J. W., Bringolf, R. B., & Tuberville, T. D. (2017). Accumulation of coal combustion residues and their immunological effects in the yellow-bellied slider (*Trachemys scripta scripta*). *Environmental Pollution*, *224*, 810–819. https://doi.org/10.1016/j.envpol.2017.01.048

Huang, C., Wei, H.-L., Rau, J.-Y., & Jhan, J.-P. (2019). Use of principal components of UAV-acquired narrow-band multispectral imagery to map the diverse low stature vegetation fAPAR. *GIScience & Remote Sensing*. https://www.tandfonline.com/doi/abs/10.1080/15481603.2018.1550873

Jiang, N., Li, Z., Yang, J., & Zu, Y. (2022). Responses of antioxidant enzymes and key resistant substances in perennial ryegrass (Lolium perenne L.) to cadmium and arsenic stresses. *BMC Plant Biology*, *22*(1), 145. https://doi.org/10.1186/s12870-022-03475-2

Kacprzak, M., Grobelak, A., Grosser, A., & Prasad, M. N. V. (2014). Efficacy of Biosolids in Assisted Phytostabilization of Metalliferous Acidic Sandy Soils with Five Grass Species. *International Journal of Phytoremediation*, *16*(6), 593–608. https://doi.org/10.1080/15226514.2013.798625

Koo, B.-J., Barton, C., & Adriano, D. (2006). Evaluation of Bahiagrass (Paspalum notatum) as a Vegetative Cover for a Landfill Containing Coal Combustion Waste. In K. S. Sajwan, I. Twardowska, T.

Punshon, & A. K. Alva (Eds.), *Coal Combustion Byproducts and Environmental Issues* (pp. 225–231). Springer. https://doi.org/10.1007/0-387-32177-2_25

Lassalle, G., Fabre, S., Credoz, A., Dubucq, D., & Elger, A. (2020a). Monitoring oil contamination in vegetated areas with optical remote sensing: A comprehensive review. *Journal of Hazardous Materials*, *393*, 122427. https://doi.org/10.1016/j.jhazmat.2020.122427

Lassalle, G., Fabre, S., Credoz, A., Dubucq, D., & Elger, A. (2020b). Monitoring oil contamination in vegetated areas with optical remote sensing: A comprehensive review. *Journal of Hazardous Materials*, *393*, 122427. https://doi.org/10.1016/j.jhazmat.2020.122427

Lichtenthaler, H. K., & Babani, F. (2022). Contents of photosynthetic pigments and ratios of chlorophyll a/b and chlorophylls to carotenoids (a+b)/(x+c) in C_4 plants as compared to C_3 plants. *Photosynthetica*, *60*(SPECIAL ISSUE 2022), 3–9. https://doi.org/10.32615/ps.2021.041

Madhu, Sharma, A., Kaur, A., Tyagi, S., & Upadhyay, S. K. (2023). Glutathione Peroxidases in Plants: Innumerable Role in Abiotic Stress Tolerance and Plant Development. *Journal of Plant Growth Regulation*, *42*(2), 598–613. https://doi.org/10.1007/s00344-022-10601-9

Matichenkov, V. (Ed.). (2017). *Phytoremediation: Methods, management and assessment*. Nova Science Publishers.

Meharg, A. A., & Hartley-Whitaker, J. (2002). Arsenic uptake and metabolism in arsenic resistant and nonresistant plant species. *New Phytologist*, *154*(1), 29–43. https://doi.org/10.1046/j.1469-8137.2002.00363.x

Milton, N. M., Ager, C. M., Eiswerth, B. A., & Power, M. S. (1989). Arsenic- and selenium-induced changes in spectral reflectance and morphology of soybean plants. *Remote Sensing of Environment*, *30*(3), 263–269. https://doi.org/10.1016/0034-4257(89)90068-0

Mishra, P., Lohumi, S., Ahmad Khan, H., & Nordon, A. (2020). Close-range hyperspectral imaging of whole plants for digital phenotyping: Recent applications and illumination correction approaches.

Computers and Electronics in Agriculture, *178*, 105780. https://doi.org/10.1016/j.compag.2020.105780

Neupane, K., & Baysal-Gurel, F. (2021). Automatic Identification and Monitoring of Plant Diseases Using Unmanned Aerial Vehicles: A Review. *Remote Sensing*, *13*(19), Article 19. https://doi.org/10.3390/rs13193841

Petrović, M., & Fiket, Ž. (2022). Environmental damage caused by coal combustion residue disposal: A critical review of risk assessment methodologies. *Chemosphere*, *299*, 134410. https://doi.org/10.1016/j.chemosphere.2022.134410

Pettorelli, N., Vik, J. O., Mysterud, A., Gaillard, J.-M., Tucker, C. J., & Stenseth, N. Chr. (2005). Using the satellite-derived NDVI to assess ecological responses to environmental change. *Trends in Ecology & Evolution*, *20*(9), 503–510. https://doi.org/10.1016/j.tree.2005.05.011

Pudasainee, D., Kurian, V., & Gupta, R. (2020). 2 - Coal: Past, Present, and Future Sustainable Use. In T. M. Letcher (Ed.), *Future Energy (Third Edition)* (pp. 21–48). Elsevier. https://doi.org/10.1016/B978-0-08-102886-5.00002-5

QGIS Development Team. (2024). *QGIS Geographic Information System*. QGIS Association. https://www.qgis.org

R Core Team. (2023). *R: A Language and Environment for Statistical Computing*. R Foundation for Statistical Computing. https://www.R-project.org/

Rafiq, M., Shahid, M., Abbas, G., Shamshad, S., Khalid, S., Niazi, N. K., & Dumat, C. (2017). Comparative effect of calcium and EDTA on arsenic uptake and physiological attributes of *Pisum sativum*. *International Journal of Phytoremediation*, *19*(7), 662–669. https://doi.org/10.1080/15226514.2016.1278426

Ruhl, L., Vengosh, A., Dwyer, G. S., Hsu-Kim, H., Schwartz, G., Romanski, A., & Smith, S. D. (2012). The Impact of Coal Combustion Residue Effluent on Water Resources: A North Carolina Example. *Environmental Science & Technology*, *46*(21), 12226–12233. https://doi.org/10.1021/es303263x

Sage, R. F., De Melo Peixoto, M., Friesen, P., & Deen, B. (2015). C_4 bioenergy crops for cool climates, with special emphasis on perennial C_4 grasses. *Journal of Experimental Botany*, *66*(14), 4195–4212. https://doi.org/10.1093/jxb/erv123

Singhal, G., Bansod, B., Mathew, L., Goswami, J., Choudhury, B. U., & Raju, P. L. N. (2019). Estimation of Leaf Chlorophyll Concentration in Turmeric (Curcuma longa) Using High-Resolution Unmanned Aerial Vehicle Imagery Based on Kernel Ridge Regression. *Journal of the Indian Society of Remote Sensing*, *47*(7), 1111–1122. https://doi.org/10.1007/s12524-019-00969-9

Somagattu, P., Chinnannan, K., Yammanuru, H., Reddy, U. K., & Nimmakayala, P. (2024). Selenium dynamics in plants: Uptake, transport, toxicity, and sustainable management strategies. *Science of The Total Environment*, *949*, 175033. https://doi.org/10.1016/j.scitotenv.2024.175033

Sun, Z., Wang, X., Wang, Z., Yang, L., Xie, Y., & Huang, Y. (2021). UAVs as remote sensing platforms in plant ecology: Review of applications and challenges. *Journal of Plant Ecology*, *14*(6), 1003–1023. https://doi.org/10.1093/jpe/rtab089

Talukder, S. K., & Saha, M. C. (2017). Toward Genomics-Based Breeding in C3 Cool-Season Perennial Grasses. *Frontiers in Plant Science*, *8*, 1317. https://doi.org/10.3389/fpls.2017.01317

Thomas, S., Behmann, J., Steier, A., Kraska, T., Muller, O., Rascher, U., & Mahlein, A.-K. (2018). Quantitative assessment of disease severity and rating of barley cultivars based on hyperspectral imaging in a non-invasive, automated phenotyping platform. *Plant Methods*, *14*(1), 45. https://doi.org/10.1186/s13007-018-0313-8

Thorneloe, S., Kosson, D., Connolly, K., & Rodgers, M. (2017). *Leaching Environmental Assessment Framework (LEAF) How-To Guide—Understanding the LEAF Approach and How and When to Use*

It (No. EPA/600/R-16/097). U.S. Environmental Protection Agency. https://www.epa.gov/sites/default/files/2019-05/documents/final_leaching_environmental_assessment_framework_leaf_how-to_guide.pdf

Umar, A. W., Naeem, M., Hussain, H., Ahmad, N., & Xu, M. (2025). Starvation from within: How heavy metals compete with essential nutrients, disrupt metabolism, and impair plant growth. *Plant Science*, *353*, 112412. https://doi.org/10.1016/j.plantsci.2025.112412

U.S. EPA. (1996). *Method 3050B: Acid Digestion of Sediments, Sludges, and Soils* (No. Revision 2).

U.S. EPA. (2024). *Fact Sheet: Legacy Coal Combustion Residuals Surface Impoundments and CCR Management Units Final Rule. Office of Resource Conservation and Recovery.* (No. EPA-530-F-24-011). chrome-extension://efaidnbmnnnibpcajpcglclefindmkaj/https://www.epa.gov/system/files/documents/2024-04/legacy_ccrmu_final-_fact_sheet_april2024.pdf

Walsh, L. M., Sumner, M. E., & Keeney, D. R. (1977). Occurrence and distribution of arsenic in soils and plants. *Environmental Health Perspectives*, *19*, 67–71. https://doi.org/10.1289/ehp.771967

Wickham, H. (2016). *ggplot2: Elegant Graphics for Data Analysis*. Springer-Verlag New York. https://ggplot2.tidyverse.org

Zhao, F. J., Ma, J. F., Meharg, A. A., & McGrath, S. P. (2009). Arsenic uptake and metabolism in plants. *New Phytologist*, *181*(4), 777–794. https://doi.org/10.1111/j.1469-8137.2008.02716.x

Zierold, K. M., & Odoh, C. (2020). A review on fly ash from coal-fired power plants: Chemical composition, regulations, and health evidence. *Reviews on Environmental Health*, *35*(4), 401–418. https://doi.org/10.1515/reveh-2019-0039

Zwolak, I. (2020). The Role of Selenium in Arsenic and Cadmium Toxicity: An Updated Review of Scientific Literature. *Biological Trace Element Research*, *193*(1), 44–63. https://doi.org/10.1007/s12011-019-01691-w

Supplementary Files

This is a list of supplementary files associated with this preprint. Click to download.

- SupplementalFiguresaerialimagingofgrassesforbiomonitoringresubmission.docx